

Unusual Radar Anomalous Propagation Associated with Foehn Winds Induced by Typhoon Krosa (2007)

Pao-Liang Chang and Pin-Fang Lin
Meteorological Satellite Center,
Central Weather Bureau

Abstract

Unusual radar anomalous propagation (AP) phenomena associated with foehn winds induced by typhoon Krosa (2007) were documented by using radar, surface stations and sounding data in this study. The AP echoes were embedded within rainband areas of typhoon Krosa and exhibited inward motions toward the radar site within 2–3 hours prior to the foehn winds occurred in the vicinity of radar site in the eastern–central part of Taiwan.

Significant subsidence warming and drying from downslope winds were found below the mountain tops as typhoon Krosa located in the vicinity of northeastern coast of Taiwan, which provided favorably environmental conditions for the occurrences of AP echoes. With the calculations of refractive index, it was found that the ducting conditions were directly correlated with the inversion heights which dominated the occurrences of AP echoes. When the foehn winds occurred, the ducting conditions were consequentially replaced with sub-refraction conditions due to the inversion height is lower than the radar height. By using ray tracing techniques, the occurrences and inward movements of AP echoes could be reasonably simulated with various inversion heights.

Key word: Anomalous propagation, foehn winds

1. Introduction

Foehn winds are typically associated with large temperature increases and relative humidity decreases due to the adiabatic compression of downslope wind, which frequently occurred on the lee sides of mountain ranges all over the world, including the chinook winds east of the Rocky Mountains (Oard 1993), foehn winds near the Appalachian Mountains of the eastern United States (Gaffin 2009), “bora” (or also “bura”) west of the Dinaric Alps (Drechsel and Mayr 2008), and “zonda” downstream of the Andes (Seluchi et al. 2003), and so on.

Taiwan, a mountainous island, is characterized by the Central Mountain Range (CMR) running across most of it in a north-northeast to south-southwest orientation (Fig. 1). With an average elevation of more than 2000 m and the highest peak close to 4000 m in the CMR, typhoons often have a profound interaction with the complex terrain and produce not only strong winds and heavy rainfalls lead to significant losses of properties and human lives, but also the foehn winds on the downwind side of the mountains lead to the agricultural losses each year (Chen et al. 2009). As northwestward or westward moving typhoons passed across the eastern or northeastern coast of Taiwan, the foehn winds frequently occurred in the southeastern and northwestern regions of Taiwan due to the strong downslope winds (Shieh et al. 1996; Wu and Kuo 1999; Chen et al. 2009).

During the passage of typhoon Krosa (2007) across Taiwan (Fig. 1), the significant foehn winds

phenomena occurred in the eastern–central to southeastern part of Taiwan. The pronounced radar anomalous propagation (AP) echoes were observed just prior to the occurrences of foehn winds, which were frequently related to the presence of ducting conditions that are associated with the environments of strong vertical gradients of temperature and humidity.

In the current study, the radar AP echoes associated with the pre-foehn winds environments will be investigated, which were not frequently documented in past studies, especially in typhoon environments. Based on surface and sounding data, the characteristics and temporal evolutions of sudden warming and drying induced by typhoon Krosa are analyzed, and the beam path trajectories (Doviak and Zrnic 1993) according to different thermodynamic environments in the lower troposphere are also examined. In the next section, the data and methodology will be described. The foehn wind phenomenon and the associated impact on radar observations are given in Section 3. A discussion and brief conclusion will be followed in section 4 and 5.

2. Data and methodology

a. Data overview

More than 200 automatically meteorological stations from Central Weather Bureau (CWB) and other government agencies were used to provide the observing parameters including temperature (T) and wind speed and direction over Taiwan Island, in which 36 surface stations also included dew-point temperature (T_d) and

pressure observations. These surface data were gathered to analyze the surface characteristics during foehn winds period. Radiosonde observations from station Hualien (46699) were utilized to analyze the thermodynamic conditions in the atmosphere and calculate the vertical refractivity index associated with the propagation of radar signals.

The Hualien (RCHL) Doppler radar from Taiwan radar network implemented by CWB of Taiwan (Fig. 1) was primarily used to investigate the AP phenomena occurred in offshore area of eastern Taiwan. Because of RCHL situates close to (~ 10 km) the foothill of the eastern side of the CMR, electromagnetic wave emissions are turned off for some sectors (Chang et al. 2009) to avoid interfered returns directly from the topography.

b. Ray tracing

Based on the equivalent earth model decried in Doviak and Zrnic (1993), procedures with stepwise calculations were established to simulate the beam path trajectories according to different thermodynamic environments in the lower troposphere (Fornasiero et al. 2006), especially for varied inversion heights or depths. In this study, the ray-tracing will be carried out by directly calculating the integral equation (1) as follows (Doviak and Zrnic 1993):

$$r(h) = \int_0^h \frac{(a+h)n^2(h)}{\left[(a+h)^2 n^2(h) - (a+h_0)^2 n^2(h_0) \cos^2 \theta_e \right]^{1/2}} dh \quad \dots (1)$$

here a is the earth's radius (meter), h is height of radar beam above sea level (meter) (ASL). $r(h)$ is the radar-measurable range, h_0 is the radar height ASL (meter), θ_e is the antenna elevation angle, and $n(h)$ and $n(h_0)$ is the refractivity index at altitude of beam and radar, respectively. The procedures for the calculations of ray paths are: (a) Calculate the refractivity index with one meter increment starting at h_0 by following equation (1). (b) The sign will be changed as the value of square bracket of the denominator in equation (1) is negative, and the sign of the increment of ray height will also be changed, which allows the equation to handle the ray ducting conditions. (c) Finally, the ray path can be carried out by integrating piecewise ranges obtained from consecutive heights in Eq. (1).

3. Results

a. Overview of typhoon Krosa

Typhoon Krosa (2007) reached its peak intensity at 0000 UTC 05 October with an estimated maximum sustained wind of 51 m s^{-1} (10-min-averaged wind), while typhoon Krosa located approximately 900 km east of Taiwan (not shown). As typhoon Krosa approached northeastern coast of Taiwan, continuous radar coverage of the eyewall and the inner rainbands was captured by RCHL radar. Radar reflectivities revealed that the typhoon Krosa eye exhibited a sharp southward turn and slow cyclonic loop off the eastern coast of Taiwan

between 0600 UTC and 1400 UTC 6 October (Fig. 1) and made landfall at 1500 UTC in the northeastern tip of Taiwan. Similar to the Typhoon Haitang (2005), the loop track was possibly contributed by the terrain-induced channeling effect (Jian and Wu 2008).

b. Surface variations

Between 0400 UTC to 0800 UTC, the temperature distributions that the distinctly warm regions were found within confined areas located in the eastern-central to southeastern Taiwan (not shown). Subsequently, areas for temperatures greater than 34°C in southeastern Taiwan extended northwardly toward eastern-central Taiwan with a maximum temperature of above 38°C at 0600 UTC (not shown). In contrast, the temperatures were no significant variations in other areas except slightly warming with a value of about 2°C in at Ilan Plain of northeastern Taiwan (not shown). As typhoon Krosa moved southwestward and closed gradually to the eastern coastline of Taiwan, the warming areas gradually moved northwardly and the maximum temperature reached above 39°C while the warming mitigated in southeastern Taiwan (Fig. 2). After the typhoon center moved along a north-south track off the east coast of Taiwan (the typhoon track during 0600–0900 UTC in Fig. 1), the warming was much more alleviative in eastern-central to southeastern Taiwan (not shown).

Located in plain area of western side of the CMR, the Taichung station (46749) shows the least variations among the four stations in temperature (T) and dew-point temperature (T_d) between 0000 UTC and 1200 UTC on 6 October 2007 (not shown). Stations on at the lee sides of the CMR show the significant variations, at about 0300 UTC, suddenly warming (about $28\text{--}36^\circ\text{C}$ in T) and drying (about $5\text{--}15^\circ\text{C}$ in $T-T_d$) began and sustained more than 9 hours at Taitung (46766) (not shown). The degrees of warming and drying conformed to the criteria defined in Shieh et al. (1996) for foehn wind phenomenon during the typhoon days, one is the $T \geq 28^\circ\text{C}$ and the other one is $T-T_d \geq 6^\circ\text{C}$. Two hours later (0500 UTC), foehn wind occurred at Chenggong (46761) located on southeastern side of Coastal Range (CR) and lasted for about 6 hours. The warming and drying were more significant than at Taitung with a maximum T and $T-T_d$ of approximate 38°C and 20°C between 0700 UTC and 0800 UTC. The foehn wind phenomenon was also found at far northern station Hualien (46699) (Fig. 3), whereas the period lasted for only about 1.5 hours beginning at 0630 UTC.

At 0800 UTC, the minimum central pressure was with an observed a, 950 hPa. when typhoon Krosa was closest to northeastern coast of Taiwan as shown in Fig. 1, It is noticeable that the wind directions veered to the southwesterly and westerly (northeasterly) when the foehn phenomenon occurred (terminated) at stations Hualien and Chenggong, revealing that warming and

drying air were possibly caused by the downslope wind which came from the mountain tops of the CMR.

c. Environmental conditions

Figure 4 shows the sounding profiles launched at Hualien at 0600 UTC on 6 October 2007. Significant subsidence warming and drying were found between surface and 700 hPa and more remarkable warming and drying as compared with the profiles at 0000 UTC (not shown). The $T-T_d$ between surface and 700 hPa reached to a maximum value of approximately 15 °C and a temperature in the inversion increased from 25 °C to 31 °C with increasing height, where the wind directions veered clockwise from south to northwesterly. The southwesterly winds near surface layer in both sounding could be dominated by the topography, however the wind which possessed westerly component at upper layers at 0600 UTC when was close to foehn winds occurred probably be influenced by the circulation of typhoon Krosa to generate the downslope wind on the lee side of the CMR.

d. Radar observations

A near circular typhoon with a radius of approximately 25 km located in northeastern direction of radar with a range of about 100 km could be found at 0505 UTC (not shown). The relatively scatter echoes were present at south-southeastern direction of radar centered at a range of about 100 km with a maximum value greater than 55 dBZ. The scattered echoes continuously move northward and another similar scattered echoe could be found in southeastern direction centered at range of about 75 km with a maximum reflectivity value of above 65 dBZ (not shown).

During typhoon Krosa's center moved along a north-south track off the east coast of Taiwan, the scattered echoes kept moving toward the radar site at ranges between 50 and 75 km (Fig 5) and characterized by an arc shape. Under horizontally uniform ducting environments, a ring shape of echoes would be observed on radar elevation observation (Fornasiero et al. 2006) At 0635 UTC (not shown), the intensity and areas size of scattered echoes reduced as typhoon Krosa eye made landfall.

4. Discussions

a. Ducting effects

Shown in Fig. 4, the sounding profiles indicated the subsidence warming and drying below 3000 m in altitude, which were likely caused by the downslope winds. The lapse rate of T and T_d between 600 m and 3000m were near constant with a value of approximately 7.5 °C km⁻¹ in T and 1.7 °C km⁻¹ in T_d (Fig. 6), which is less than the dry adiabatic lapse rate 9.8 °C km⁻¹ in T . It's implied that the diabatic process including evaporations or mixing may contribute to the decrease of lapse rate during air parcels descended. From an increasing rate of about 1 g kg⁻¹ km⁻¹ of mixing ratio with decreasing

height from T_d profile in the environment, that would produce a cooling rate, about 2.3 °C km⁻¹, during the air parcels descended (Rogers and Yau 1989). After the dry adiabatic lapse rate was added, the net lapse rate of T is approximately 7.5 °C km⁻¹ that is consistent with lapse rate between 600 m and 3000 m as shown in Fig. 6.

Fig. 7 shows the beam paths under the sounding profile at Hualien at 0600 UTC on 6 October 2007 (Fig. 4), and the 3 dB main lobes of radar beams below 0.5 degrees elevation angle were also considered. For elevation angles lower than 0.2 degrees, the ray paths propagated downward toward the surface and showed the ducting features with wavelength of approximately 250 km and amplitudes of approximately 50–75 m. In contrast, the ray paths propagated upward smoothly for elevation angles greater than or equal 0.2 degrees but the beam heights with increasing range were still lower than normal propagation conditions (not shown). The beam-splitting features were found between 0.1 and 0.2 degrees known as "radio hole" as described in Fornasiero et al. (2006), which would distort drastically the integration volume assumed in normal propagation conditions making very difficult to retrieve the real density distribution and the observed volume. The ducting features of simulated ray paths below 0.1 degrees generally agreed with the occurrences of AP echoes at ranges between 100 and 140 km near southern direction of the RCHL radar (not shown).

b. Inversion heights

In order to investigate the moving characteristics of AP echoes, the T and T_d profiles (Fig. 6) based on the Hualien sounding observation at 0600 UTC on 6 October 2007 were modified to examine the ray paths (Fig. 7). As aforementioned, the air parcels in the foehn winds were assumed that they came from the downslope winds, the idealized vertical profiles, A–F profiles, were constructed based on the lapse rates of T and T_d and the inversion heights. Profiles A to F represented the inversion heights lowered from 300 m to 50 m with an interval of 50 m. To examine the effects of ray ducting according to different inversion heights, the elevation angle of radar beam was examined at 0.1 degree as shown in Fig 7. Fig. 8 shows pronounced features of ducting phenomena were between inversion heights 100 m and 250 m, and the ducting amplitudes were around 25–50 m. When the inversion heights decreased from 250 m to 100 m, the wavelengths shortened from about 125 km to 50 km. The results indicated that the AP echoes associated with ducting conditions could move inwardly toward the radar when the inversion heights decreased.

When the inversion height was assumed at 50 m, the ray path dramatically went upward, because the inversion height was lower than the radar height (63 m), which would cause the super-refraction phenomenon for the radar electromagnetic waves. As documented in Lopez (2009), increasing the installation height of

ground-based radars that may reduce the frequency of the ducting conditions, because the steepest refractivity gradients are generally confined within tens of meters in height (e.g., Babin et al. 1997). However, tall towers indicated that the clutter under normal conditions can be increased as a result of undesirable contributions from the side lobes emitted by the antenna (Doviak and Zrnic 1993). Consequentially, the choice of the proper radar height should eventually be a compromise between all of these competing benefits and drawbacks (Lopez 2009).

5. Conclusions

As typhoon Krosa (2007) moved along a north-south track off the east coast of Taiwan, the foehn winds with significant subsidence warming (a maximum T 38 °C) and drying (a maximum $T-T_d$ 20 °C) generated by downslope winds were observed, and continuously moved northwardly within confined areas from the southeast to eastern-central part of Taiwan. Within 2–3 hours prior to the foehn winds occurred in the vicinity of radar site in the eastern-central part of Taiwan, the radar AP echoes were found to be embedded within typhoon Krosa's rainband areas and appeared an inward motion toward the radar site.

These results revealed that the pre-foehn winds environments induced by typhoon could potentially provide favorable conditions for the occurrences of radar ducting so that might cause the contamination in precipitation echoes, reductions in the radar signals, range-height errors. It is shown that the occurrences of ducting conditions and associated AP phenomena could be adequately accessed if the sounding observations are available in real-time operation.

Acknowledgements: The authors would like to thank Central Weather Bureau for providing the analyzed data and computer resource. This research is supported by the National Science Council of Taiwan, Republic of China, under Grant 98-2625-M-052-005-.

Reference

Babin, S. M., 1996: Surface duct height distribution for Wallop Island, Virginia, 1985–1994, *J. Appl. Meteorol.*, **35**, 86–93.

———, G. S. Young, and J. A. Carton, 1997: A new model of the oceanic evaporation duct. *J. Appl. Meteor.*, **36**, 193–204.

Chang, P. L., P. F. Lin, B. J.-D. Jou, and J. Zhang, 2009: An application of reflectivity climatology in constructing radar hybrid scans over complex terrain. *J. Atmos. Oceanic Technol.*, **26**, 1315–1327.

Chen, T. C., S. Y. Wang, M. C. Yen, A. J. Clark, and J. D. Tsay, 2009: Sudden surface warming/drying events caused by typhoon passages across Taiwan. *J. Appl. Meteor. Climatol.* (in press)

Doviak, R. J., and D. S., Zrnic, 1993: *Doppler radar and weather observations*, Academic Press, 562 pp.

Drechsel, S., and G. J. Mayr, 2008: Objective forecasting of foehn winds for a subgrid-scale Alpine valley. *Wea. Forecasting*, **23**, 205–218.

Fornasiero, A., P. P. Alberoni, and J. Bech, 2006: Statistical analysis and modelling of weather radar beam propagation in the Po Valley (Italy). *Nat. Hazards Earth Syst. Sci.*, **6**, 303–314.

Gaffin, D. M., 2009: On high winds and foehn warming associated with mountain-wave events in the western foothills of the southern Appalachian mountains. *Wea. Forecasting*, **24**, 53–75.

Jian, G. J., and C. C. Wu, 2008: A numerical study of the track deflection of supertyphoon Haitang (2005) prior to its landfall in Taiwan. *Mon. Wea. Rev.*, **136**, 598–615.

Lin, Y. L., D. B. Ensley, S. Chiao, and C. Y. Huang, 2002: Orographic influences on rainfall and track deflection associated with the passage of a tropical cyclone. *Mon. Wea. Rev.*, **130**, 2929–2950.

Lopez, P., 2009: A 5-yr 40-km-resolution global climatology of superrefraction for ground-based weather radars. *J. Appl. Meteor. Climatol.*, **48**, 89–110.

Oard, M. J., 1993: A method for predicting chinook winds east of the Montana Rockies. *Wea. Forecasting*, **8**, 166–180.

Seluchi, M. E., F. A. Norte, P. Satyamurty, and S. C. Chou, 2003: Analysis of three situations of the foehn effect over the Andes (zonda wind) using the Eta-CPTec regional model. *Wea. Forecasting*, **18**, 481–501.

Rogers, R. R., and M. K. Yau, 1989: A short course in cloud physics. 3d ed. Pergamon Press, 293 pp.

Shieh, S. L., S. T. Wang, M. D. Cheng, and T. C. Yeh, 1996: User's guide (1) for typhoon forecasting in the Taiwan area (in Chinese). Res. Rep. CWB84-1M-01, 356 pp.

Wu, C. C. and Y. H. Kuo, 1999: Typhoons affecting Taiwan: Current understanding and future challenges. *Bull. Amer. Meteor. Soc.*, **80**, 67–80.

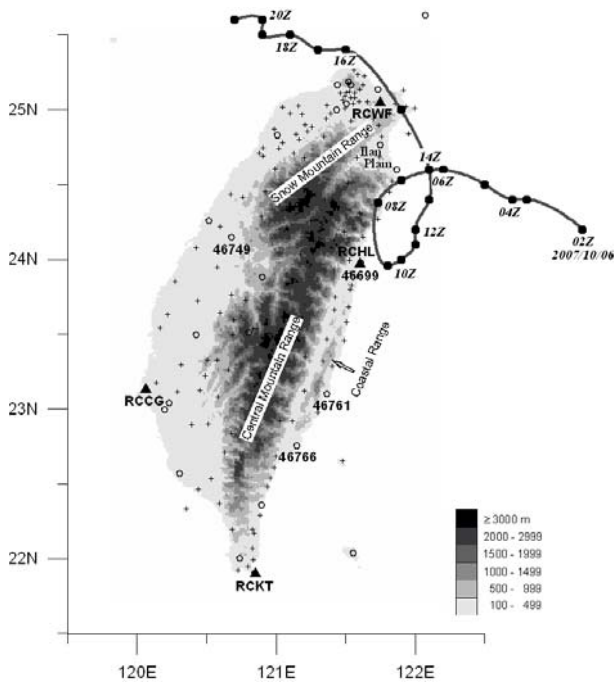


FIG. 1. Distributions of observation stations in Taiwan. Gray shades represent the terrain heights. Locations of radar sites are marked with the abbreviations. Surface and automatic meteorological stations are denoted by open circle symbols and plus symbols, respectively. The typhoon track determined by radar reflectivity is also indicated.

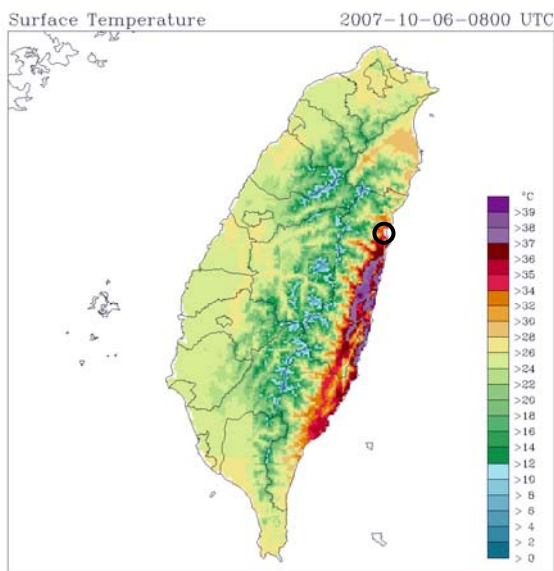


FIG. 2. Distributions of hourly temperature ($^{\circ}\text{C}$) at 0800 UTC on 6 October 2007. The location of Hualien radar site is denoted by open circle symbol.

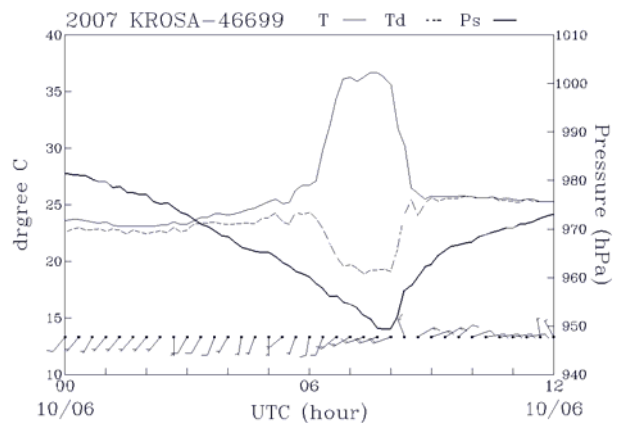


FIG. 3. Temporal evolutions of temperature ($^{\circ}\text{C}$) (solid line), dew-point temperature ($^{\circ}\text{C}$) (dash line), and pressure (hPa) (heavy solid line) at station 46699 (Hualien) between 0000 UTC and 1200 UTC on 6 October 2007. Full-wind barbs correspond to 10 m s^{-1} and half barbs correspond to 5 m s^{-1} .

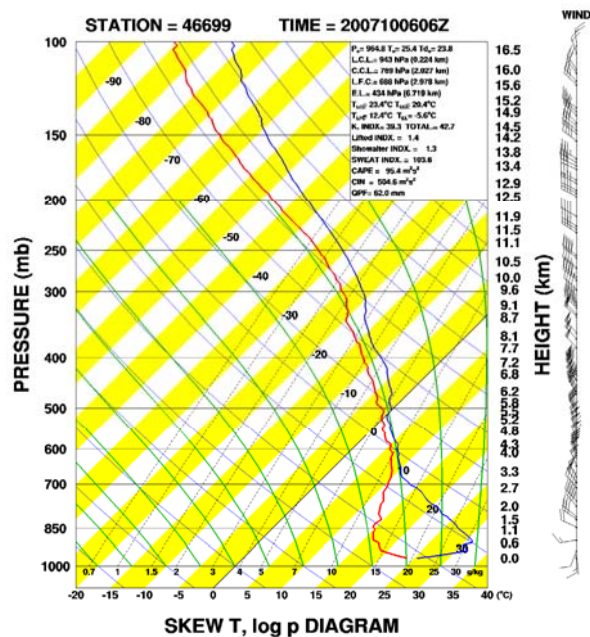


FIG. 4. Hualien sounding launched at 0600 UTC on 6 October 2007. Winds are in knots. Full-wind barbs correspond to 5 m s^{-1} and half barbs correspond to 2.5 m s^{-1} .

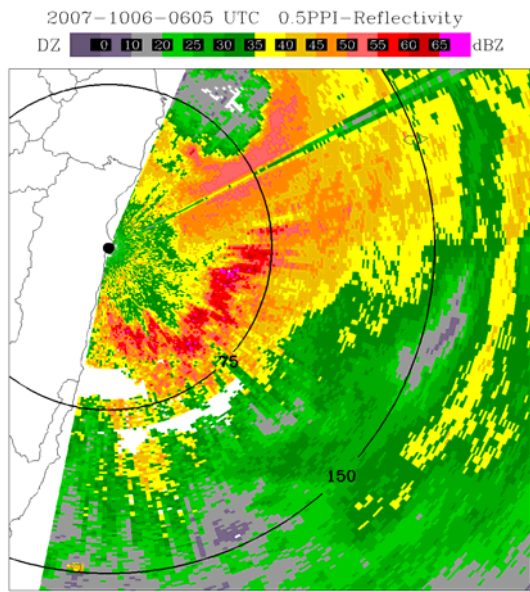


FIG. 5. RCHL base reflectivities at 0.5° elevation from Typhoon Krosa at 0605 UTC on 6 October 2007. Range rings of 75 and 150 km centered at radar site RCHL are also indicated.

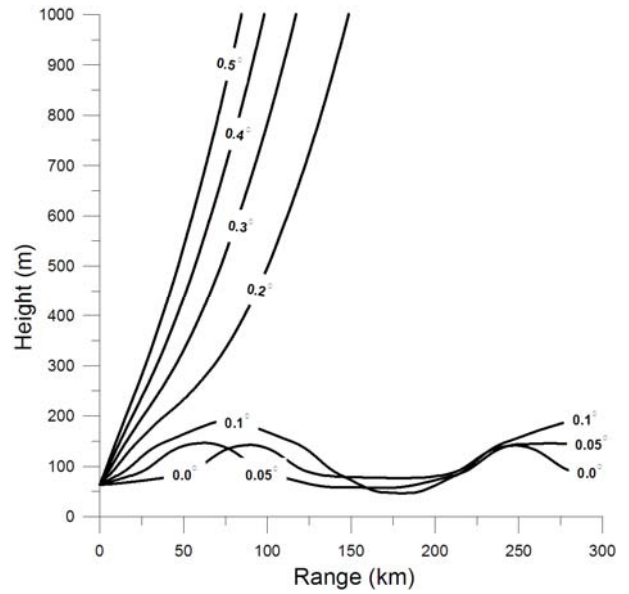


FIG. 7. The radar ray paths relative to the RCHL radar from elevations 0 to 0.5 degrees by using the calculations of refractivity index and ray tracing based on the sounding profile at 0600 UTC on 6 October 2007.

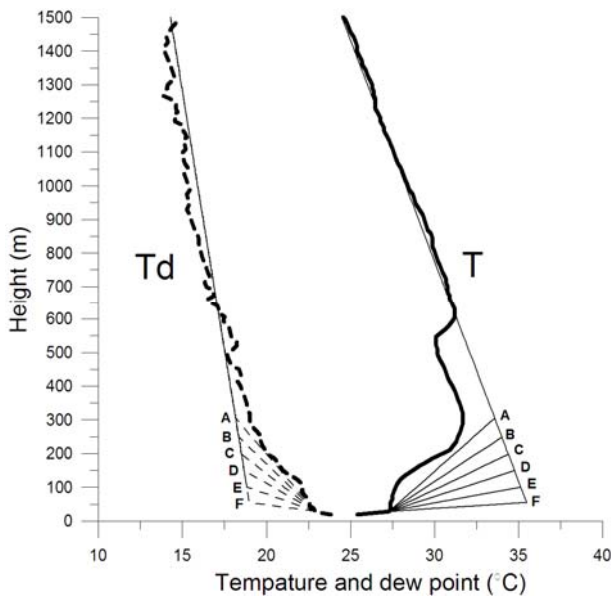


FIG. 6. Vertical profiles of temperature (T, heavy solid line) and dew-point (Td, heavy dash line) from Hualien sounding at 0600 UTC on 6 October 2007. Idealized inversion profiles of T and Td from A to F are used for the simulations of ray paths in Fig. 8.

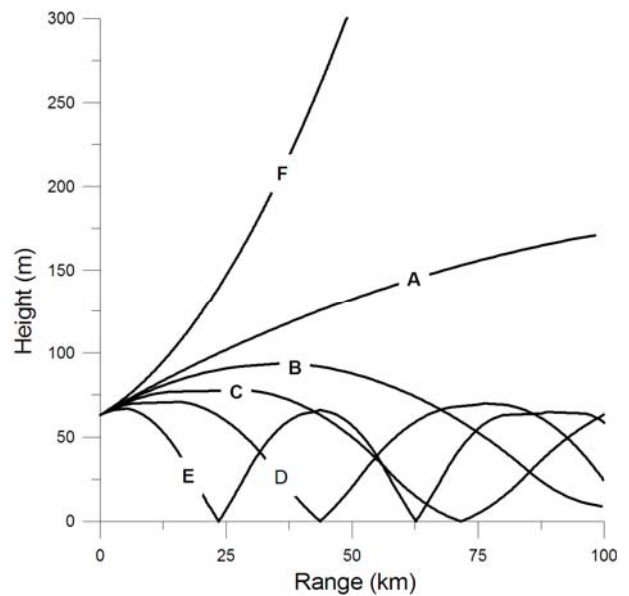


FIG. 8. Same as Fig 7, expect for the radar ray paths at elevation 0.1 degrees from idealized vertical inversion profiles from A to F with different inversion heights as indicated in Fig. 6.